Int. J. Oral Maxillofac. Surg. 2019; 48: 302–308
https://doi.org/10.1016/j.ijom.2018.08.015, available online at https://www.sciencedirect.com

International Journal of Oral & Maxillofacial Surgery

Research Paper
Craniofacial Anomalies

Describing the mandible in patients with craniofacial microsomia based on principal component analysis and thin plate spline video analysis

O. Kaya[1,2,a], B. I. Pluijmers[1,a], F. Staal[2], C. Ruff[1], B. L. Padwa[3], M. J. Koudstaal[1,2,3], D. J. Dunaway[1]
[1]The Craniofacial Unit, Great Ormond Street Hospital, London, UK; [2]The Dutch Craniofacial Centre, Department of Oral and Maxillofacial Surgery, Erasmus University Medical Centre, Sophia's Children's Hospital, Rotterdam, the Netherlands; [3]Department of Oral and Maxillofacial Surgery, Boston Children's Hospital, Boston, Massachusetts, USA

O. Kaya, B. I. Pluijmers, F. Staal, C. Ruff, B. L. Padwa, M. J. Koudstaal, D. J. Dunaway: Describing the mandible in patients with craniofacial microsomia based on principal component analysis and thin plate spline video analysis. Int. J. Oral Maxillofac. Surg. 2019; 48: 302–308.

Abstract. Craniofacial microsomia (CFM) is most often described as a unilateral malformation of derivatives of the first and second branchial arches. The mandible has been classified using several classification systems. However, all are based on two-dimensional imaging. The aim of this study was to mathematically describe the deformed mandible based on principal component analysis (PCA) in a three-dimensional way. This may aid in defining the flaws in existing surgical corrections of the mandible through the identification of the differences in shape compared with a normal mandible in a holistic view with the help of videos. Forty-three homologous landmarks were defined to describe a mandible with CFM. Computed tomography scans of 22 patients and 30 controls were marked manually. The changes in shape between the mandibles were visualized using videos. A lateral rotation with increase in posterior rotation of the condyle due to shortening of the condyle–gonial height and a longitudinal rotation with outward bending of the mandibular angle were noted on the affected side, as well as an inward bending of the angle on the unaffected side. Due to the compensatory remodelling of the mandible on the unaffected side, one could suggest that CFM is never truly unilateral.

Key words: craniofacial microsomia; hemifacial microsomia; mandibular correction; mandibular surgery; geometric morphometrics; principal component analysis.

Accepted for publication 2 August 2018
Available online 15 September 2018

Craniofacial microsomia (CFM) is a complex congenital anomaly that is characterized by an underdevelopment of derivatives of the first and second branchial arches. It is estimated to occur in 1:3500 to 1:20,000 live births, which makes it the second most common craniofacial disorder following cleft lip and palate[1–3]. Although it is most often regarded as a unilateral malformation,

[a] O. Kaya and B. I. Pluijmers contributed equally to this paper.

0901-5027/030302 + 07

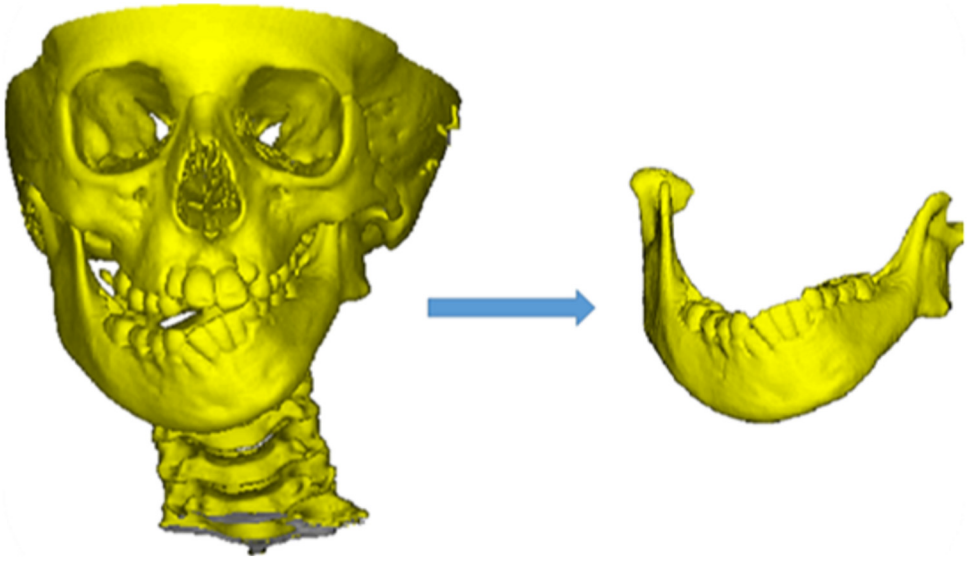

Fig. 1. The mandible was isolated manually from the rest of the craniofacial skeleton if delineation of the condyles and coronoid process was possible from the articulating glenoid fossa.

the involvement of clinical features is bilateral in 10% of the cases[4–6]. However, asymmetry is commonly observed even in the bilateral cases. Structures involved include, among others, the mandible, orbit, zygoma, maxilla, ears, soft tissue, and facial nerves. The phenotype can range from subtle facial asymmetry or microtia to severe underdevelopment of the structures mentioned above.

Mandibular hypoplasia is often the most striking deformity in CFM and occurs in 89–100% of affected patients[7]. The heterogeneous presentation of CFM challenges the classification of deformity. With regard to the mandible, the severity of hypoplasia can be classified into the following four types based on the Pruzansky–Kaban classification: type I, referring to minimal hypoplasia of the mandible; type IIa, referring to abnormal shape and size of the mandibular ramus; type IIb, referring to a hypoplastic mandibular ramus and a temporomandibular joint (TMJ) abnormal in morphology and position; type III, referring to an absent ramus, condyle, and TMJ[8,9]. However, it must be noted that the Pruzansky–Kaban classification is based on two-dimensional (2D) imaging, i.e. cephalograms and panoramic radiographs, thus three-dimensional (3D) information is lost. Furthermore, the Pruzansky–Kaban classification currently tends to show inter- and intra-rater variability in the evaluation of affected mandibles[10].

Geometric morphometrics is a mathematical modelling technique that uses homologous anatomical landmark points to convert the skull into a geometric object with Cartesian coordinates[11]. Homologous landmarks are necessary and need to be accurate and reliable to validate geometric morphometrics modelling. The landmarks should be reliable and easy to repeat; furthermore there should be sufficient landmarks to represent the specific shape. Intersections of sutures, foramina, and recognizable ridges are often used[11,12]. Landmarks represent the coordinates of specific points on the surfaces, and the space between them is interpolated. Principal component analysis (PCA) can be applied to landmarks placed on the mandible and can be used to evaluate the variation in shape change between mandibles within a CFM population and between a CFM and control population.

PCA has previously been used in the analysis of craniofacial shapes in anthropological studies and has also been shown to be useful in characterizing hard tissue deformities of Apert, Crouzon, and Pfeiffer skulls and more recently to describe the CFM skull base[13–15]. PCA and geometric morphometrics make it possible to visualize shape change in a 3D way. This could be helpful in improving the surgical planning for the correction of craniofacial deformities by identifying the flaws in current surgical techniques.

The aim of this study was to obtain a better understanding of the variance in shape in CFM patients in order to possibly help refine the current treatment modalities. At the same time, it was sought to assess the efficacy of PCA in the characterization of mandibular deformity in CFM.

Methods

Data collection

The craniofacial databases of three craniofacial units in three countries were used to identify CFM patients: Great Ormond Street Hospital, London, UK (GOSH), Erasmus Medical Centre, Rotterdam, the Netherlands (EMC), and Boston Children's Hospital, Boston, USA (BCH).

CFM patients with a unilateral presentation, between the ages of 6 and 19 years, and for whom good quality preoperative 3D computed tomography (CT) scans were available, were included. Patients with a Pruzansky–Kaban type III mandible were excluded due to the lack of homologous points over the deformity.

An age-matched control group was recruited, which included the CT scans of patients with anatomically normal skulls. The data were collected from a series of trauma patients undergoing diagnostic CT scans at EMC and from a series of epileptic patients undergoing CT scans for surgical planning at GOSH. Inclusion criteria were patients with an unaffected facial skeleton, between the ages of 6 and 19 years.

The scans were obtained in DICOM format (Digital Imaging and Communications in Medicine) using a 16-slice Siemens Somatom Sensation spiral CT scanner set to 0.75-mm collimation (Siemens AG, Munich, Germany). DICOM data were reconstructed into polygon mesh surfaces (stereolithography, STL) demonstrating bone and then loaded into a mesh viewer (Robin's 3D Voxel Ren-

Table 1. Landmarks.

Landmark	Position	Definition
A	Infradentale	Most anterosuperior point on the labial crest of the mandibular alveolar process
B	B-point	Most posterior point of the bony curvature of the mandible below infradentale and above pogonion
C	Pogonion	Most anterior point on the mandible in the midline
D	Menton	The most inferior point of the mandibular symphysis
E	Right mental tubercle	Most anterolateral aspect of the right mental tubercle
F	Left mental tubercle	Most anterolateral aspect of the left mental tubercle
G	Right digastric fossa	Greatest curvature right of menton
H	Left digastric fossa	Greatest curvature left of the menton
I	Right mental foramen	Most anteromedial point of the right mental foramen
J	Left mental foramen	Most anteromedial point of the left mental foramen
K	Right mid-mandibular point	Most protruding part of the right ramus beneath molar 2
L	Left mid-mandibular point	Most protruding part of the left ramus beneath molar 2
M	Right retromolar fossa	Marker in the middle of the area behind the last molar
N	Left retromolar fossa	Marker in the middle of the area behind the last molar
O	Right anterior ramus (negative)	Point in the middle of the anterior border of the right ramus
P	Left anterior ramus (negative)	Point in the middle of the anterior border of the right ramus
Q	Right mandibular notch	Point of greatest concavity on the right mandibular notch
R	Left mandibular notch	Point of greatest concavity on the left mandibular notch
S	Linguale	Most posterior point on the posterior aspect of symphysis
T	Right linguale curve	Greatest curvature right of the linguale point
U	Left linguale curve	Greatest curvature left of the linguale point
V	Right mylohyoid line	Most posterior point on the right mylohyoid line
W	Left mylohyoid line	Most posterior point on the left mylohyoid line
X	Right lingula	Most posterior point of right lingula
Y	Left lingula	Most posterior point of left lingula
Z	Right gonion	Point on the right mandibular angle representing the intersection of the lines of the posterior ramus and the inferior border of the mandible
A1	Left gonion	Point on the left mandibular angle representing the intersection of the lines of the posterior ramus and the inferior border of the mandible
B1	Right coronion	Most superior point on the right coronoid process
C1	Left coronion	Most superior point on the left coronoid process
D1	Right pterygoid fovea	Point of maximum curvature within the right pterygoid fovea
E1	Left pterygoid fovea	Point of maximum curvature within the left pterygoid fovea
F1	Right condylion lateralis	Most lateral aspect of the right condylar head
G1	Left condylion lateralis	Most lateral aspect of the left condylar head
H1	Right condylion medialis	Most medial aspect of the right condylar head
I1	Left condylion medialis	Most medial aspect of the left condylar head
J1	Right condylion superioris	Most superior aspect of the right condylar head
K1	Left condylion superioris	Most superior aspect of the left condylar head
L1	Right condylion posterioris	Most posterior aspect of the right condylar head
M1	Left condylion posterioris	Most posterior aspect of the left condylar head
N1	Right condylion anterioris	Most anterior aspect of the right condylar head
O1	Left condylion anterioris	Most anterior aspect of the left condylar head
P1	Right medial condylar neck	Point of most negative curvature beneath right condylion medialis
Q1	Left medial condylar neck	Point of most negative curvature beneath left condylion medialis

dering Software, London, United kingdom, 2015) for segmenting and landmarking.

In total 22 CFM patients were included: nine from GOSH in London, five from EMC in Rotterdam, and eight from BCH in Boston. A total of 30 controls were included. The CFM patients were divided into two age groups to lessen the dilution effects of allometric growth: 6–12 years ($n = 13$) and 13–19 years ($n = 9$). The controls were stratified into two corresponding groups: 6–12 years ($n = 14$) and 13–19 years ($n = 16$).

To guarantee unbiased shape analysis, all prevalent left-sided defects were mirrored before landmarking. The mandible was isolated from the rest of the craniofacial skeleton to gain access to all regions in order to correctly place the necessary landmarks (Fig. 1). The segmentation and landmarking was performed manually using Robin 3D software if delineation of the condyles and coronoid process was possible from the articulating glenoid fossa.

Landmarks

Based on anatomy and existing anthropometric points, 43 landmarks were considered (Table 1, Fig. 2). The landmarks were more densely located around the condyles in order to be able to fully capture these geometrically complex regions. The landmarks were validated with the help of colour map algorithms (Fig. 3). If the landmarks are distributed adequately over the mandibular surface and the morphology is captured sufficiently well, the colour map will show very little difference between surfaces. The aim was to ensure that this was the case, particularly in the regions known to be affected in CFM, such as the coronoid processes, condyles, and rami.

A random control and CFM mandible were chosen and landmarked 10 times in

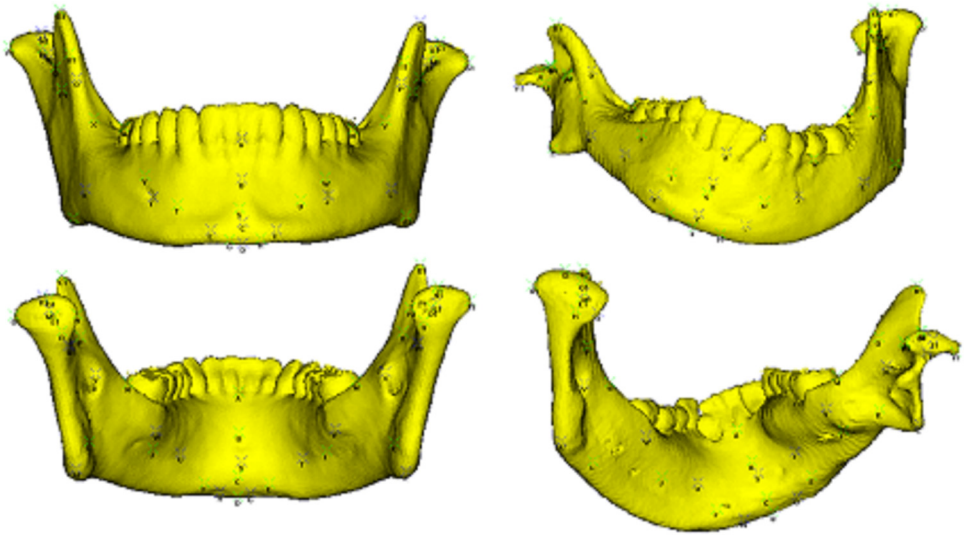

Fig. 2. A control (left) and CFM mandible (right) with the 43 landmarks placed on the surfaces (Table 1).

different sittings to determine the landmark repeatability and intra-observer reliability. The standard deviation (SD) was calculated to determine intra-observer reliability for all 43 landmarks. Finally, another random control mandible was chosen and landmarked 10 times in different sittings by two researchers based at different locations. Subsequently the inter-observer reliability for each landmark was determined by performing a *t*-test and reading the *P*-values.

Shape analysis

PCA is able to quantify the differences in shape within a population by reducing the dimensionality of the shape data into lesser amounts of variables, called principal components or modes of variation. This analysis is done using a point distribution model (PDM). A PDM is a model that describes the mean shape and the variability allowed within a population. PDMs describe the variation between the spatial relationships of the landmarks. After placing the landmarks, the software documented the Cartesian coordinates of each landmark. A shape defined by a series of landmarks can be represented by one point in a multidimensional space. The shape difference of the principal components is calculated from the eigenvectors of the covariance matrix[12]. The resulting modes of variation representing the principal components are ordered such that the first mode describes the

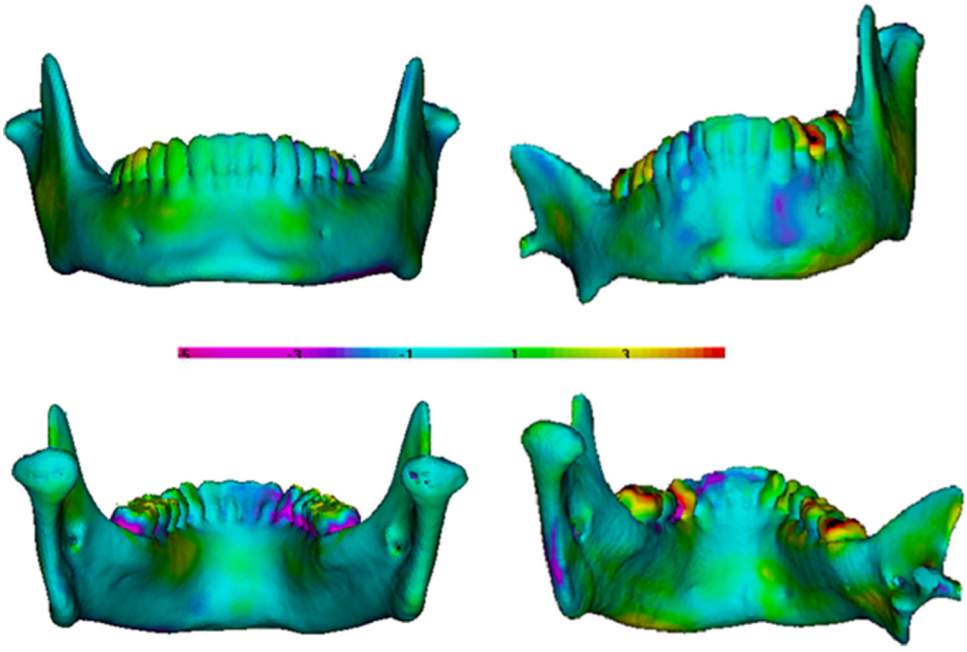

Fig. 3. The colour map algorithm showing the difference in surfaces between randomly chosen control mandibles (left) and randomly chosen CFM mandibles (right). The colour maps use a range of 5 mm to demonstrate positive and negative surface differences. Light blue areas indicate good correspondence with less than 1 mm difference. (For interpretation of the references to colour in this figure legend, the reader is referred to the web version of this article.)

Table 2. Shape variation within the craniofacial microsomia group and control group according to the mode of variation.

Mode of variation	Craniofacial microsomia	Controls
First mode	6–12 years: allometric growth • Receded chin • Shorter, more horizontal and inward bending body/ramus • Smaller condylar process 13–19 years: • Rotation and shortening of condylar process • Unaffected side: biplanar rotation of body and coronoids	Allometric growth Both age groups: • More prominent body • Condylar lengthening
Second mode	Both age groups: • Angulation of lateral body on affected side • Rotation of anterior mandibular body • Unaffected side: involvement, causing a narrower jaw	6–12 years: • Ramus widening and vertical growth 13–19 years • Pronounced chin cleft associated with narrow ramus and more anterior coronoids
Third mode	6–12 years: • Narrower chin • Lateral splaying of the ramus • Unaffected side: anterior rotation 13–19 years: • Angulation of lateral body • Unaffected side: rotation of body	6–12 years: • Chin shape variation • Body shape variation 13–19 years: • Chin shape variation • Body length variation

biggest difference within the population and each subsequent mode represents the remaining variability associated with shape variations decreasing in prevalence.

Thin plate spline (TPS) warping uses minimum bending energy and interpolates changes between landmarks to estimate the surface between these points[11]. This technique was able to visualize the changes by creating movies that showed variation within and among the different groups. To study the changes in shape, movie sequences were created by interpolating the mandibles over 32 frames. An average mandible for each group was warped to the landmarks of the mean CFM/normal mandible, thereby visualizing the shape change between the CFM and control population. Furthermore, the mean CFM/normal mandible was warped to −2 SD and +2 SD along each mode of variation, thereby visualizing the shape change within the population.

Results

Landmarks

Generally, the colour maps showed good congruity between the surfaces, indicating that the landmarks were satisfactory in capturing the mandibular morphology of the CFM and control populations. Essentially, the complex regions most affected in CFM such as the coronoid processes and condyles all showed a difference in surface of not much more than 1 mm. The overall good level of congruity between surfaces, most importantly in the affected regions, justified the use of the set of 43 landmarks for both the CFM and control populations.

None of the landmarks used exceeded a SD of more than 3 mm. For both populations, landmarks placed on anatomically distinct areas such as the mental foramen showed greater reliability than landmarks placed on areas such as curves.

For the control mandibles, 40 out of 43 landmarks were within the threshold of a SD less than 1 mm. Three of the landmarks used showed a SD between 1 mm and 2 mm. Therefore 93% of the landmarks were considered very reliable for the control population and none of the landmarks exceeded the 2 mm limit.

With regard to the reliability for the CFM mandibles, 41 out of the 43 landmarks were within the threshold of a SD less than 1 mm. One of the landmarks used showed an SD between 1 mm and 2 mm and one showed an SD between 2 mm and 3 mm. Thus, 95% of the landmarks were considered very reliable for the CFM population and only one landmark exceeded the 2 mm limit.

The inter-observer variability for the chosen control mandible showed a significant difference for 38 out of the 43 landmarks ($P < 0.05$). For the two researchers, 88% of the landmarks were placed in significantly different areas, with a smallest significant distance difference of 0.23 mm (placed on the left digastric fossa) and the largest significant distance difference being 3.98 mm (placed on the right lingual curve).

Shape analysis

CFM patients

The first mode of variation showed allometric growth in the younger population. For both the older group and younger group, smaller mandibles were associated with a receded chin and a shorter, more horizontal lateral body/ramus that bends inwards, with a smaller condylar process. The more severe phenotype was found to be associated with small size and a shape change at the chin and angle of the jaw. In the younger group, there was found to be no shape change to the unaffected side. In the older group, the unaffected side showed biplanar rotation of the body and coronoid process, with rotation and shortening of the condylar process associated with a less prominent angle and greater severity of the affected side. The rotation of the unaffected side compensated for the growth of the affected side.

In the second mode of variation, there was involvement of the unaffected side in both the younger and older age groups. A narrower jaw caused by greater rotation of the unaffected side and greater angulation of the lateral body on the affected side was seen. Similarly there was rotation of the anterior (unaffected) mandibular body (**Supplementary Material**, video 1).

In the third mode of variation, lateral splaying of the ramus on the affected side associated with anterior rotation of the ramus on the unaffected side and a narrower chin was observed in the younger population. With regard to the older patients with CFM, again a rotation of the unaffected side and greater angulation of the lateral body on the affected side causing a narrow jaw overall was seen. However, the chin appeared not to be affected (Table 2).

Control group

The first mode of variation showed allometric growth in both age groups. In the older group, the videos showed lengthening of the condylar processes associated with prominence of the angle and an increased height of the body, with the jaw becoming squarer and taller.

The second mode of variation showed widening of the ramus from the midline in the youngest group. There was an increase in height of the anterior body, upper angulation of the lateral body, and descent of the chin. A longer chin was associated with a narrower jaw (angles nearer the midline) and vice versa, i.e., vertical growth. In the older group, a more pronounced chin cleft – a dent in the region of the symphysis – was associated with a narrow ramus towards the midline and forward placement of the coronoid processes.

For the younger population, the third mode of variation showed variations in chin shape from a sharper chin, associated with a longer body and more anterior coronoid process, to a round chin. Chin variation and jaw length dominated, similar to the second mode for the older controls. For the older population, a narrow jaw was associated with a longer chin (inferior descent) and taller coronoid processes. Chin and jaw width variation dominated, mimicking the second mode for the younger controls (Table 2).

CFM to control

Most allometric growth was cancelled out. Shape changes were seen between the mandible of CFM patients and the unaffected mandible. The videos showed a lengthening of the height of the mandibular body and ramus. It was found that the less affected the mandible becomes, the greater the decrease in outward rotation of the mandibular angle on the affected side. Furthermore, lengthening of the condyles and coronoid processes was seen going from CFM to normal. However, there was a greater increase in condyle–gonion height than coronoid–gonion height, leading to lesser posterior angulation of the ramus. There was an overall increase in size of the affected side. The unaffected side showed outward rotation similar to the inward rotation of the affected side. Also, there was chin displacement to the affected side (**Supplementary Material**, video 2) (Table 3).

Discussion

The aim of this study was to mathematically describe the CFM mandible in a holistic way to increase understanding of the deformity in order to refine current (surgical) treatment modalities.

Most of the conclusions of this study are based on anatomy and visual description rather than measurable data. However, the data obtained were based on an objective description of the output visuals produced by this complex mathematical model, thereby providing quantitative information. Although the mathematical output of PCA may be challenging to understand from a clinician's point of view, when visualized anatomically, the information becomes highly functional and valuable.

PCA is a mathematical tool and does not specifically take anatomy into account; therefore it is crucial to validate the results using anatomical knowledge of the mandible. The first mode of variation in the control population largely showed allometric growth and the subsequent modes increasingly demonstrated normal variation. This is expected, because allometric growth is very likely to contribute more towards overall variation than subtler differences in morphology, as seen in the later modes. Therefore, by being in tandem with what is expected from the growing mandible, the modes of variation validate the PCA model and allow confident conclusions to be drawn from it. Based on earlier studies, three principal components were used[13–15]. As stated above, the first principal component is mostly allometric growth, which was seen in both the control and CFM patients groups. Therefore the second and third modes of variation are the most descriptive with regard to the actual change in morphology. After the third mode of variation, the morphology changes are too subtle to differ from the second and third.

The placement of the landmarks is a crucial but time-consuming process. Although the intra-observer reliability was good due to the learning curve, the assessment of inter-observer reliability showed a significant difference in distance ranging from 0.23 mm to 3.98 mm ($P < 0.05$) for 38 of the 43 points. Not surprisingly, the greatest inter-observer differences in distance were seen for the 'smooth' surfaces of the mandible and the smallest differences were seen for the anatomical landmarks such as the fossae and foramina.

The aetiology of CFM is possibly related to a disturbed migration of the neural crest, leading to underdevelopment of the structures of the first and second branchial arches[16]. The mandible, a derivative of the first branchial arch, is possibly the most reported feature of CFM[6,10,17]. The mandibular hypoplasia and heterogeneous phenotype represent a challenge for surgery aimed at correcting the asymmetry. Furthermore, as demonstrated by the videos, although one side most often seems to be more dominant in CFM, the unaffected side tends to be affected due to compensatory remodelling of the mandible. As described previously, development in one region may affect the entire craniofacial skeleton[18–21]. This would suggest that a patient with CFM is never truly affected unilaterally. Along with this concept is the influence of the underdevelop-

Table 3. Shape change between the craniofacial microsomia group and control group.

	CFM to control
Overall	• Less allometric growth • Affected side: size increase and inward rotation • Unaffected side: outward rotation
Body	• Height increase • Chin displacement to the affected side
Ramus	• Height increase • Lesser posterior angulation
Condyles and coronoids	• Lengthening • Condyle–gonion height shows a greater increase than coronoid–gonion height

CFM, craniofacial microsomia.

ment of the mandible with the other structures of the viscerocranium.

Recent work by Schaal et al. showed significant asymmetry of the skull base in CFM, with the most significant asymmetries and restrictions of growth centred around the glenoid fossa and mastoid process[13]. Distortion of the skull in this area is complex and is present in the vertical, horizontal, and antero-posterior planes, associated with a rotation of this part of the skull base. This concept suggests that with the increase in hypoplasia of the skull base, an increase in distortion is seen, which has an effect on the growth of structures in the same region, such as the temporal bone, possibly leading to posterior displacement of the condyle[16]. Several studies have already demonstrated that the maxilla and orbit become displaced secondary to the lack of mandibular growth on the affected side[18–21]. Therefore, the present authors are currently working on a study that combines the different areas of the CFM skull: the mandible, maxilla/midface, and skull base.

In conclusion, shape analysis based on PCA allows a mathematical description of the shape of a deformed mandible in 3D. The holistic nature of thin plate spline warping, derived from the PCA, allows a review of the shape change, which helps in understanding the actual changes in shape and may possibly aid in the refinement of current (surgical) treatment strategies.

A CFM mandible differs from a normal mandible as a result of hypoplasia leading to a rotation towards the affected side; there is both a lateral rotation with increase of posterior rotation of the condyle due to shortening of the condyle–gonial height and a longitudinal rotation with outward bending of the mandibular angle on the affected side, as well as inward bending of the angle on the unaffected side. Due to the compensatory remodelling of the mandible on the unaffected side, one could suggest that CFM is never truly unilateral.

Funding

None.

Competing interests

None.

Ethical approval

This study was approved by the R&D Medical Ethics Review Committee Great Ormond Street Hospital for Sick Children (file number 14 DS25); the Medical Ethics Review Committee of Erasmus Medical Centre (file number MEC-2013-575); and by the IRB Medical Ethics Review Committee of Boston Children's Hospital (file number X05-08-058).

Patient consent

Not required.

Appendix A. Supplementary data

Supplementary data associated with this article can be found, in the online version, at https://doi.org/10.1016/j.ijom.2018.08.015.

References

1. Grabb WC. The first and second branchial arch syndrome. *Plast Reconstr Surg* 1965;**36**:485–508.
2. Melnick M. The etiology of external ear malformations and its relation to abnormalities of the middle ear, inner ear, and other organ systems. *Birth Defects Orig Artic Ser* 1980;**16**:303–31.
3. Poswillo D. Otomandibular deformity: pathogenesis as a guide to reconstruction. *J Maxillofac Surg* 1974;**2**:64–72.
4. Posnick JC, Ruiz RL, Tiwana PS. Craniofacial dysostosis syndromes: stages of reconstruction. *Oral Maxillofac Surg Clin North Am* 2004;**16**:475–91.
5. Ross RB. Lateral facial dysplasia (first and second branchial arch syndrome, hemifacial microsomia). *Birth Defects Orig Artic Ser* 1975;**11**:51–9.
6. Caron C, Pluijmers BI, Wolvius EB, Looman CW, Bulstrode N, Evans RD, Ayliffe P, Mulliken JB, Dunaway D, Padwa B, Koudstaal MJ. Craniofacial and extracraniofacial anomalies in craniofacial microsomia: a multicenter study of 755 patients. *J Craniomaxillofac Surg* 2017;**45**:1302–10.
7. Heike CL, Luquetti DV, Hing AV. Craniofacial microsomia overview. In: Adam MP, Ardinger HH, Pagon RA, Wallace SE, Bean LJH, Stephens K, Amemiya A, eds.: GeneReviews [Internet] Seattle, WA: University of Washington, 1993–2018. 2009 Mar 19 [updated 2014 Oct 9].
8. Pruzansky S. Not all dwarfed mandibles are alike. *Birth Defects Orig Artic Ser* 1969;**5**:120–9.
9. Kaban LB, Moses MH, Mulliken JB. Correction of hemifacial microsomia in the growing child: a follow-up study. *Cleft Palate J* 1986;**23**(Suppl 1):50–2.
10. Birgfeld CB, Heike CL, Saltzman BS, Leroux BG, Evans KN, Luquetti DV. Reliable classification of facial phenotypic variation in craniofacial microsomia: a comparison of physical exam and photographs. *Head Face Med* 2016;**12**:14.
11. Bookstein FL. Shape and the information in medical images: a decade of the morphometric synthesis. *Comput Vis Image Underst* 1997;**66**:97–118.
12. O'Higgins P. The study of morphological variation in the hominid fossil record: biology, landmarks and geometry. *J Anat* 2000;**197**(Pt 1):103–20.
13. Schaal SC, Ruff C, Pluijmers BI, Pauws E, Looman CW, Koudstaal MJ, Dunaway DJ. Characterizing the skull base in craniofacial microsomia using principal component analysis. *Int J Oral Maxillofac Surg* 2017;**46**:1656–63.
14. Staal FC, Ponniah AJ, Angullia F, Ruff C, Koudstaal MJ, Dunaway D. Describing Crouzon and Pfeiffer syndrome based on principal component analysis. *J Craniomaxillofac Surg* 2015;**43**:528–36.
15. Pluijmers BI, Ponniah AJ, Ruff C, Dunaway D. Using principal component analysis to describe the Apert skull deformity and simulate its correction. *J Plast Reconstr Aesthet Surg* 2012;**65**:1750–2.
16. Sze RW, Paladin AM, Lee S, Cunningham ML. Hemifacial microsomia in pediatric patients: asymmetric abnormal development of the first and second branchial arches. *AJR Am J Roentgenol* 2002;**178**:1523–30.
17. Birgfeld CB, Heike C. Craniofacial microsomia. *Semin Plast Surg* 2012;**26**:91–104.
18. Kaban LB. Mandibular asymmetry and the fourth dimension. *J Craniofac Surg* 2009;**20** (Suppl 1):622–31.
19. Kaban LB, Moses MH, Mulliken JB. Surgical correction of hemifacial microsomia in the growing child. *Plast Reconstr Surg* 1988;**82**:9–19.
20. Ongkosuwito EM, van Neck JW, Wattel E, van Adrichem LN, Kuijpers-Jagtman AM. Craniofacial morphology in unilateral hemifacial microsomia. *Br J Oral Maxillofac Surg* 2013;**51**:902–7.
21. Rune B, Selvik G, Sarnas KV, Jacobsson S. Growth in hemifacial microsomia studied with the aid of roentgen stereophotogrammetry and metallic implants. *Cleft Palate J* 1981;**18**:128–46.

Address:
Britt I. Pluijmers
Department of Oral and Maxillofacial Surgery
Erasmus University Medical Centre
Sophia Children's Hospital Rotterdam's
Wytemaweg 12
3015 CN Rotterdam
the Netherlands
Tel.: +31 010 7033519
Fax: +31 010 7033098
E-mail: b.pluijmers@erasmusmc.nl